Sclerostin influences body composition by regulating catabolic and anabolic metabolism in adipocytes

Soohyun P. Kim[a,1], Julie L. Frey[a,1], Zhu Li[a], Priyanka Kushwaha[a], Meredith L. Zoch[a], Ryan E. Tomlinson[a], Hao Da[a], Susan Aja[b,c], Hye Lim Noh[d], Jason K. Kim[d,e,f], Mehboob A. Hussain[g,h,i], Daniel L. J. Thorek[j,k], Michael J. Wolfgang[c,g], and Ryan C. Riddle[a,l,2]

[a]Department of Orthopaedic Surgery, The Johns Hopkins University School of Medicine, Baltimore, MD 21205; [b]Department of Neuroscience, The Johns Hopkins University School of Medicine, Baltimore, MD 21205; [c]Center for Metabolism and Obesity Research, The Johns Hopkins University School of Medicine, Baltimore, MD 21205; [d]Program in Molecular Medicine, University of Massachusetts Medical School, Worcester, MA 01655; [e]Department of Medicine, Division of Endocrinology and Metabolism, University of Massachusetts Medical School, Worcester, MA 01655; [f]Department of Medicine, Division of Diabetes, University of Massachusetts Medical School, Worcester, MA 01655; [g]Department of Biological Chemistry, The Johns Hopkins University School of Medicine, Baltimore, MD 21205; [h]Department of Pediatrics, The Johns Hopkins University School of Medicine, Baltimore, MD 21205; [i]Department of Medicine, The Johns Hopkins University School of Medicine, Baltimore, MD 21205; [j]Division of Nuclear Medicine and Molecular Imaging, Department of Radiology and Radiologic Sciences, The Johns Hopkins University School of Medicine, Baltimore, MD 21205; [k]Cancer Molecular and Functional Imaging Program, Department of Oncology, Sidney Kimmel Comprehensive Cancer Center, The Johns Hopkins University School of Medicine, Baltimore, MD 21205; and [l]Baltimore Veterans Administration Medical Center, Baltimore, MD 21201

Edited by Clifford J. Tabin, Harvard Medical School, Boston, MA, and approved November 15, 2017 (received for review May 12, 2017)

Sclerostin has traditionally been thought of as a local inhibitor of bone acquisition that antagonizes the profound osteoanabolic capacity of activated Wnt/β-catenin signaling, but serum sclerostin levels in humans exhibit a correlation with impairments in several metabolic parameters. These data, together with the increased production of sclerostin in mouse models of type 2 diabetes, suggest an endocrine function. To determine whether sclerostin contributes to the coordination of whole-body metabolism, we examined body composition, glucose homeostasis, and fatty acid metabolism in Sost$^{-/-}$ mice as well as mice that overproduce sclerostin as a result of adeno-associated virus expression from the liver. Here, we show that in addition to dramatic increases in bone volume, Sost$^{-/-}$ mice exhibit a reduction in adipose tissue accumulation in association with increased insulin sensitivity. Sclerostin overproduction results in the opposite metabolic phenotype due to adipocyte hypertrophy. Additionally, Sost$^{-/-}$ mice and those administered a sclerostin-neutralizing antibody are resistant to obesogenic diet-induced disturbances in metabolism. This effect appears to be the result of sclerostin's effects on Wnt signaling and metabolism in white adipose tissue. Since adipocytes do not produce sclerostin, these findings suggest an unexplored endocrine function for sclerostin that facilitates communication between the skeleton and adipose tissue.

sclerostin | Wnt | bone | adipose | metabolism

Bone acquisition and homeostasis are intimately linked to nutritional status. The large numbers of osteoblasts and osteocytes that carry out and coordinate new bone formation require a steady supply of energy-rich molecules to produce the mineralized extracellular matrix that comprises skeletal tissue. When the energetic demands of these specialized cells exceed available resources, normal bone growth and accrual are greatly diminished (1, 2). Recent advances in our knowledge of the physiological functions of bone, which now extend beyond locomotion, mineral ion storage, and protection of vital organs, indicate that skeletal energy requirements are communicated by the secretion of bone-derived hormones that contribute to the coordination of whole-body metabolism (3, 4).

Sclerostin, the product of the *SOST* gene, is a secreted cysteine-knot glycoprotein with homology to the Dan domain family (5). Produced predominantly by the osteocyte, sclerostin exerts profound control over bone acquisition. This effect is exemplified by the rare bone-overgrowth conditions of sclerosteosis and van Buchem disease that result from genetic disruptions in *SOST* expression (6, 7). In vitro and genetic evidence indicate that sclerostin acts within the skeleton to restrain the potent osteoanabolic actions of Wnt/β-catenin signaling (5, 8). Sclerostin interacts with the negatively charged β-propeller domains of the low-density lipoprotein-related receptor 5 (Lrp5) and Lrp6 Wnt coreceptors (9), and thereby prevents the propagation of Wnt signals that lead to the stabilization of the downstream transcription factor β-catenin (10, 11).

Outside of the skeleton, sclerostin is present in serum, and circulating levels correlate with fracture risk (12, 13), are influenced by sex hormones (14, 15), and respond to intermittent parathyroid hormone administration (16). Several lines of circumstantial evidence raise the possibility that circulating sclerostin exerts functions beyond those associated with bone acquisition and acts systemically to influence metabolic function. First, circulating levels of sclerostin are increased in type 2 diabetics relative to healthy controls (17–19) and exhibit a positive correlation with body mass index and fat mass in diabetics as well as healthy adults (20–23). Second, a recent cross-sectional analysis (24) reported that serum sclerostin levels exhibit a positive correlation with fasting glucose production and indices of hepatic and adipose insulin resistance as well as a negative correlation with whole-body glucose disposal and insulin clearance rate. Finally, mutations in *LRP5*, particularly those that affect the interaction of sclerostin with this Wnt coreceptor (25), are associated with altered fat distribution (26). These findings imply that sclerostin influences whole-body metabolism and may do so by influencing Wnt signaling in insulin target tissues.

Significance

Sclerostin exerts profound control over skeletal metabolism by regulating the osteoanabolic Wnt/β-catenin signaling pathway. In this study, we demonstrate that in addition to a dramatic increase in bone mass, Sost$^{-/-}$ mice as well as those treated with a sclerostin-neutralizing antibody exhibit a reduction in white adipose tissue mass and are protected from high fat diet feeding. This effect is associated with an increase in fatty acid oxidation and reduced de novo fatty acid synthesis in adipocytes due to increased Wnt/β-catenin signaling.

Author contributions: S.P.K., M.J.W., and R.C.R. designed research; J.L.F., Z.L., P.K., M.L.Z., R.E.T., H.D., S.A., H.L.N., J.K.K., M.A.H., D.L.J.T., M.J.W., and R.C.R. performed research; J.K.K., M.A.H., M.J.W., and R.C.R. analyzed data; and R.C.R. wrote the paper.

The authors declare no conflict of interest.

This article is a PNAS Direct Submission.

[1]S.P.K. and J.L.F. contributed equally to this work.

[2]To whom correspondence should be addressed. Email: rriddle1@jhmi.edu.

This article contains supporting information online at www.pnas.org/lookup/suppl/doi:10.1073/pnas.1707876115/-/DCSupplemental.

Here, we report on an endocrine function of sclerostin that influences the accumulation of adipose tissue. In addition to the expected increases in bone mass, mice lacking a functional *Sost* gene develop a marked reduction in fat mass with enhanced glucose tolerance and insulin sensitivity. Sclerostin deficiency and pharmacological neutralization also confer a protective effect against the detrimental consequences of high fat diet (HFD) feeding, as mutant mice exhibited reductions in weight gain and inflammation of adipose tissue. Sclerostin overproduction produces the reverse phenotype as mice accumulate adipose tissue. Our results suggest the existence of a bone–adipose interaction, wherein sclerostin favors adipogenesis and adipose hypertrophy via the suppression of Wnt signaling and alterations in both catabolic and anabolic metabolism.

Results

Serum Sclerostin Levels Are Increased in Mouse Models of Disturbed Metabolism. The correlation of serum sclerostin levels with impairments in multiple metabolic parameters in humans (17–24) led us to consider an endocrine function for sclerostin in the coordination of metabolism. To explore this hypothesis, we initially sought to replicate findings from human studies by examining *Sost* gene expression and serum sclerostin levels in mouse models of disturbed metabolism. In the first study, cohorts of male C57BL/6 mice were fed a high fat diet (60% of calories from fat) or isocaloric control diet for up to 8 wk. As expected, high fat diet feeding resulted in an increase in body weight and fat pad mass (*SI Appendix*, Fig. S1 *A* and *B*) as well as the development of hyperglycemia, hyperinsulinemia, and osteopenia (*SI Appendix*, Fig. S1 *C–I*). These phenotypes were accompanied by significant increases in both *Sost* mRNA levels in the femur and circulating sclerostin levels (*SI Appendix*, Fig. S1 *J* and *K*). By contrast, serum levels of Dkk1, another Wnt signaling antagonist, were unaffected (*SI Appendix*, Fig. S1*L*), which is suggestive of a selective effect of impaired whole-body metabolism on sclerostin production. In a second study, sclerostin levels were measured in both the *ob*/*ob* and *db*/*db* mouse models and their respective littermate controls. By 6 wk of age, serum sclerostin levels were increased in both males and females of each mutant mouse strain (*SI Appendix*, Fig. S1 *M* and *N*). Together these data support a linkage between serum sclerostin levels and metabolism and the possibility that sclerostin contributes directly to the development of metabolic disease. It is unlikely that the accumulation of serum sclerostin is due to alterations in renal clearance, as the declining kidney function inherent in these models (27) should accelerate the excretion of sclerostin (28).

Fat Mass and Adipocyte Size Are Reduced in Sost$^{-/-}$ Mice. To assess the biologic significance of increased serum sclerostin in states of impaired metabolism and to formally characterize a role for sclerostin in the regulation of normal whole-body metabolism, we generated cohorts of control (Sost$^{+/+}$) and *Sost* knockout mice (Sost$^{-/-}$) and assessed body composition by qNMR and necropsy. Sost$^{-/-}$ mice exhibited the expected increases in bone mass (29) (Fig. 1 *A* and *B* and *SI Appendix*, Table S1) and had normal body weight (Fig. 1*C*), but qNMR analyses revealed significant reductions in whole-body fat mass (Fig. 1*D*) and a strong trend toward increased lean body mass fraction in older animals ($P = 0.06$, Fig. 1*E*). In accordance with these data, the weights of major white adipose depots were significantly reduced in 16-wk-old Sost$^{-/-}$ mice relative to littermate controls (Fig. 1*F*), while the weights of interscapular brown adipose and major organs remained normal (Fig. 1*G*). A similar phenotype was evident in 8-wk-old Sost$^{-/-}$ mice (*SI Appendix*, Fig. S2).

The reduced fat mass in Sost$^{-/-}$ mice was not associated with major alterations in behavior or whole body energy balance. Food intake and ambulatory activity were similar in 8-wk-old control and Sost$^{-/-}$ mice as were the oxygen consumption rate (VO_2), the respiratory exchange ratio (RER), and the rate of energy expenditure (Fig. 1*H* and *SI Appendix*, Fig. S3 *A–D*) in indirect calorimetry studies. Therefore, the change in body composition is likely due to alterations in the rate of anabolic metabolism or to changes in the oxidative metabolism in selective organs, such as white adipose tissue (WAT), that contributes minimally to whole-body energy expenditure (30–32).

Close examination of tissue structure by histological analyses suggested that sclerostin-deficiency affects adipocyte hypertrophy. In both the gonadal (gWAT) and inguinal (iWAT) adipose depots, the size of individual adipocytes was markedly reduced in Sost$^{-/-}$ mice relative to wild-type (WT) controls (Fig. 1*I* and *SI Appendix*, Fig. S4). Adipocyte size was also reduced in female Sost$^{-/-}$ mice relative to controls, but the weights of individual fat pads were not changed (*SI Appendix*, Fig. S5). Given the role of sclerostin as a Wnt signaling antagonist (5, 8) and inhibitory effects of Wnt on adipocyte development (30, 33, 34), we suspected this phenotype might be the result of increased Wnt signaling in white adipose depots. Consistent with this hypothesis, the mRNA levels of the Wnt target genes Axin2 and Nkd2 (35, 36) were significantly increased in the gonadal fat pad of Sost$^{-/-}$ mice relative to controls (Fig. 1*J*). By contrast, Smad1/5/9 phosphorylation levels (Fig. 1*K*), a marker of bone morphogenetic protein (Bmp) signaling, were significantly reduced in the gonadal fat pads of Sost$^{-/-}$ mice, suggesting that sclerostin is not acting as a BMP antagonist in this tissue (37). Hepatocyte morphology (Fig. 1*I*) and Wnt target gene expression in the liver, muscle, and pancreas of Sost$^{-/-}$ mice was comparable to that of controls (Fig. 1*L*), suggesting that the effects of sclerostin deficiency on body composition are unique to white adipose tissue.

Adeno-Associated Viral Sost Overexpression Increased Fat Mass. Since global deletion of the *Sost* gene has the potential to influence fat mass as a result of early developmental defects (38), we next examined postnatal effects of increasing circulating sclerostin levels. Cohorts of 8-wk-old C57BL/6 mice were injected with adeno-associated virus-8 constructs containing a *Sost* cDNA (AAV-Sost) or that of green fluorescent protein (AAV-GFP) to direct transgene expression from liver hepatocytes. When examined 8 wk postinjection, serum sclerostin levels were increased by more than 65% in AAV-Sost mice (Fig. 2*A*) and were on par with the levels we observed in mouse models of type 2 diabetes (*SI Appendix*, Fig. S1). As expected, increasing the levels of serum sclerostin was accompanied by modest reductions in trabecular bone mass in the femur (13.7%) and L5 vertebrae (12.3%) compared with control AAV-GFP mice (Fig. 2*B*).

The overproduction of sclerostin did not influence body weight (Fig. 2*C*), but the body composition phenotype of AAV-Sost mice was the opposite of that evident in Sost$^{-/-}$ mice. qNMR and necropsy analyses revealed an increase in whole-body fat mass, a small, but significant reduction in lean body mass fraction, and an increase in the mass of white adipose depots in AAV-Sost mice relative to AAV-GFP mice, while the weights of other organs were similar (Fig. 2 *D–G*). As with sclerostin deficiency, the increased fat mass in mice overproducing sclerostin was likely due to alterations in anabolic metabolism or small changes in oxidation over the course of the study as no major changes in behavior or whole-body energy balance were evident during indirect calorimetry analyses (Fig. 2*H* and *SI Appendix*, Fig. S3 *E–H*).

In line with the notion that sclerostin regulates adipocyte hypertrophy, adipocytes in the gonadal fat pad of AAV-Sost mice were significantly larger than those in AAV-GFP mice (Fig. 2*I*). To examine the basis for this change in morphology, we compared gene expression profiles in gonadal adipose isolated from the AAV-Sost and AAV-GFP mice. Markers of Wnt signaling were significantly reduced in AAV-Sost mice (Fig. 2*J*), but the mRNA levels of phenotypic markers of adipocyte differentiation

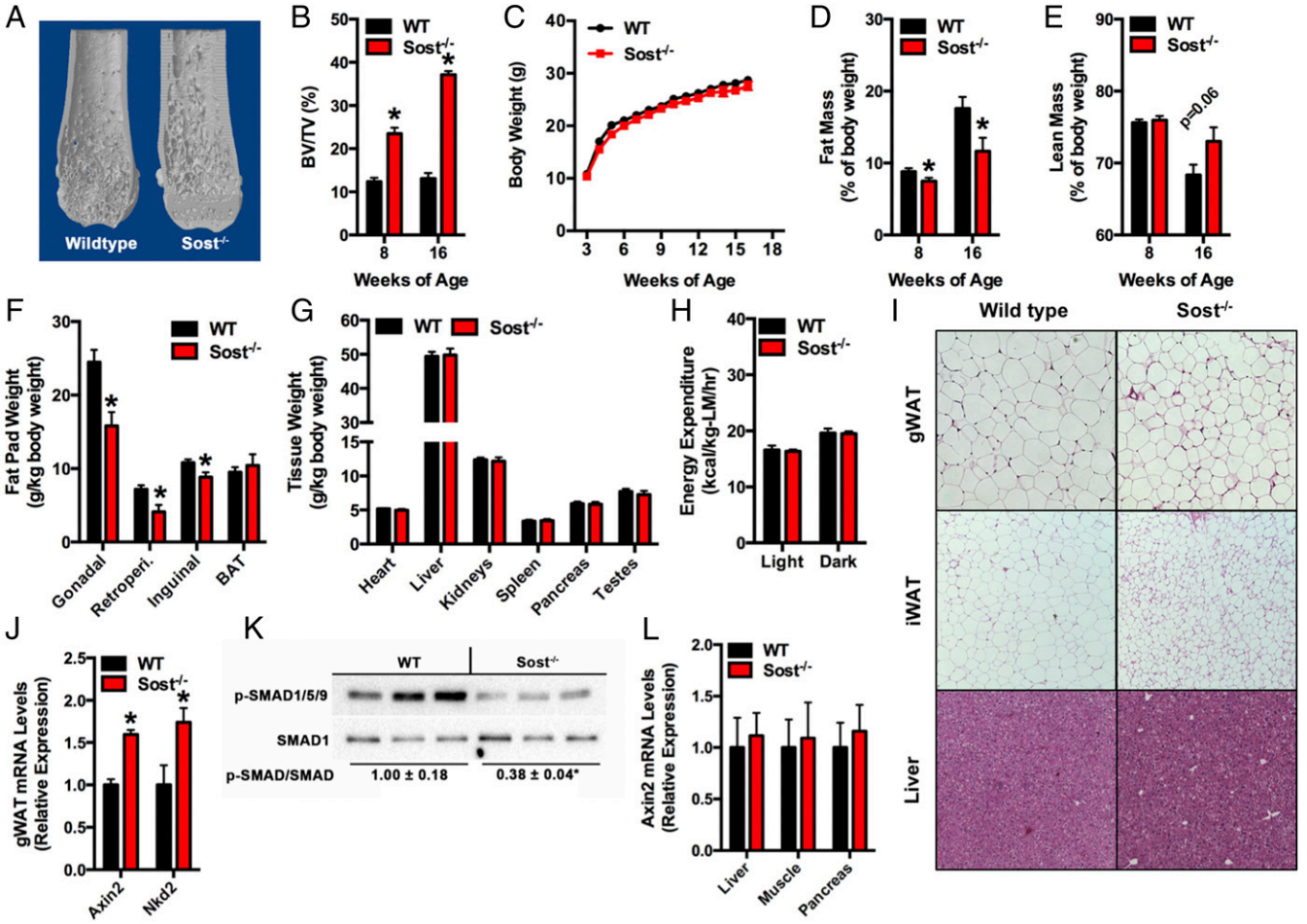

Fig. 1. Fat mass is reduced in Sost$^{-/-}$ mice. (*A*) Representative computer renderings of bone structure in the distal femur of control (WT) and Sost$^{-/-}$ mice. (*B*) Quantification of trabecular bone volume in the distal femur at 8 and 16 wk of age (n = 6–10 mice per group). (*C*) Body weight was assessed weekly (n = 6–10 mice per group). (*D* and *E*) qNMR analysis of fat mass and lean mass at 8 and 16 wk of age (n = 6–9 mice per group). (*F*) Adipose depot weights were assessed at 16 wk of age (n = 6–8 mice per group). (*G*) Wet tissue weights of major organs from WT and Sost$^{-/-}$ mice (n = 6–8 mice per group). (*H*) Energy expenditure at 8 wk of age from indirect calorimetry. Data are normalized to lean body mass (n = 6 mice per group). (*I*) Representative histological sections of gonadal (gWAT) and inguinal (iWAT) fat pads and liver from 16-wk-old WT and Sost$^{-/-}$ mice (10× magnification). (*J*) qPCR analysis of Wnt target gene expression in gWAT (n = 6 mice per group). (*K*) Immunoblot analysis of phosphorylated Smad1/5/9 levels in gWAT (n = 3 mice per group). (*L*) qPCR analysis of Axin2 expression in liver, muscle, and pancreas (n = 5 mice per group). All data are represented as mean ± SEM. *P < 0.05.

(Fig. 2*K*), including Cebpa, Fabp4, Lpl, and Pparg, were significantly increased relative to those in the white adipose of AAV-GFP mice. Similarly, the expression levels of a number of enzymes involved in de novo lipid synthesis and storage were increased in tissues isolated from AAV-Sost mice (Fig. 2*L*). The liver of AAV-Sost mice appeared normal with no evidence of steatosis (Fig. 2*M*). These data imply that sclerostin regulates body composition by facilitating adipocyte differentiation and the synthesis and/or accumulation of triglycerides.

Sclerostin Modulates Glucose Metabolism and Insulin Sensitivity. Since serum sclerostin levels are correlated with parameters of glucose homeostasis in humans (24) and adipocyte size is an indicator of adipose tissue insulin sensitivity (39, 40), we reasoned that the changes in body composition and adipocyte morphology evident in the Sost$^{-/-}$ and AAV-Sost mice might be associated with alterations in glucose metabolism. Fasting and random fed glucose levels were similar in Sost$^{-/-}$ mice relative to control littermates at 16 wk of age (Fig. 3*A*), but random fed insulin levels were significantly reduced in the *Sost* knockouts (Fig. 3*B*), which is suggestive of an increase in insulin sensitivity. In agreement with this idea, Sost$^{-/-}$ mice exhibited improvements in glucose handling during glucose tolerance and insulin tolerance tests (Fig. 3 *C*–*E*). Moreover, β-cell islet area per tissue area and mean islet size were reduced in the pancreas (Fig. 3 *F*–*H*) relative to controls, likely a secondary effect of the increased insulin sensitivity and reduced need for insulin production. Younger, 8-wk-old Sost$^{-/-}$ male mice and female mutants exhibited similar improvement in glucose handling and insulin tolerance relative to controls (*SI Appendix*, Figs. S5 and S6). To further examine insulin action in Sost$^{-/-}$ mice, we conducted 2-h hyperinsulinemic-euglycemic clamp studies in awake mice using two insulin infusion rates (1.25 mU/kg/min and 2.5 mU/kg/min, Fig. 3 *I*–*M*). In both cases, the steady-state glucose infusion rate required to maintain euglycemia (~7 mM) was significantly higher in *Sost* knockouts compared with control littermates (Fig. 3*I*), confirming the increased insulin sensitivity in the Sost$^{-/-}$ mice. Basal hepatic glucose production (HGP) rates were similar in the control and mutant mice (Fig. 3*J*), but under clamp conditions (1.25 mU/kg/min, Fig. 3*K*), a greater suppression of HGP was evident in the Sost$^{-/-}$ mice. Similarly, injection of 2-[^{14}C]-deoxyglucose during the clamp revealed a significant increase in insulin-stimulated glucose uptake in skeletal muscle in Sost knockouts at the lower insulin infusion rate (Fig. 3*L*). There was

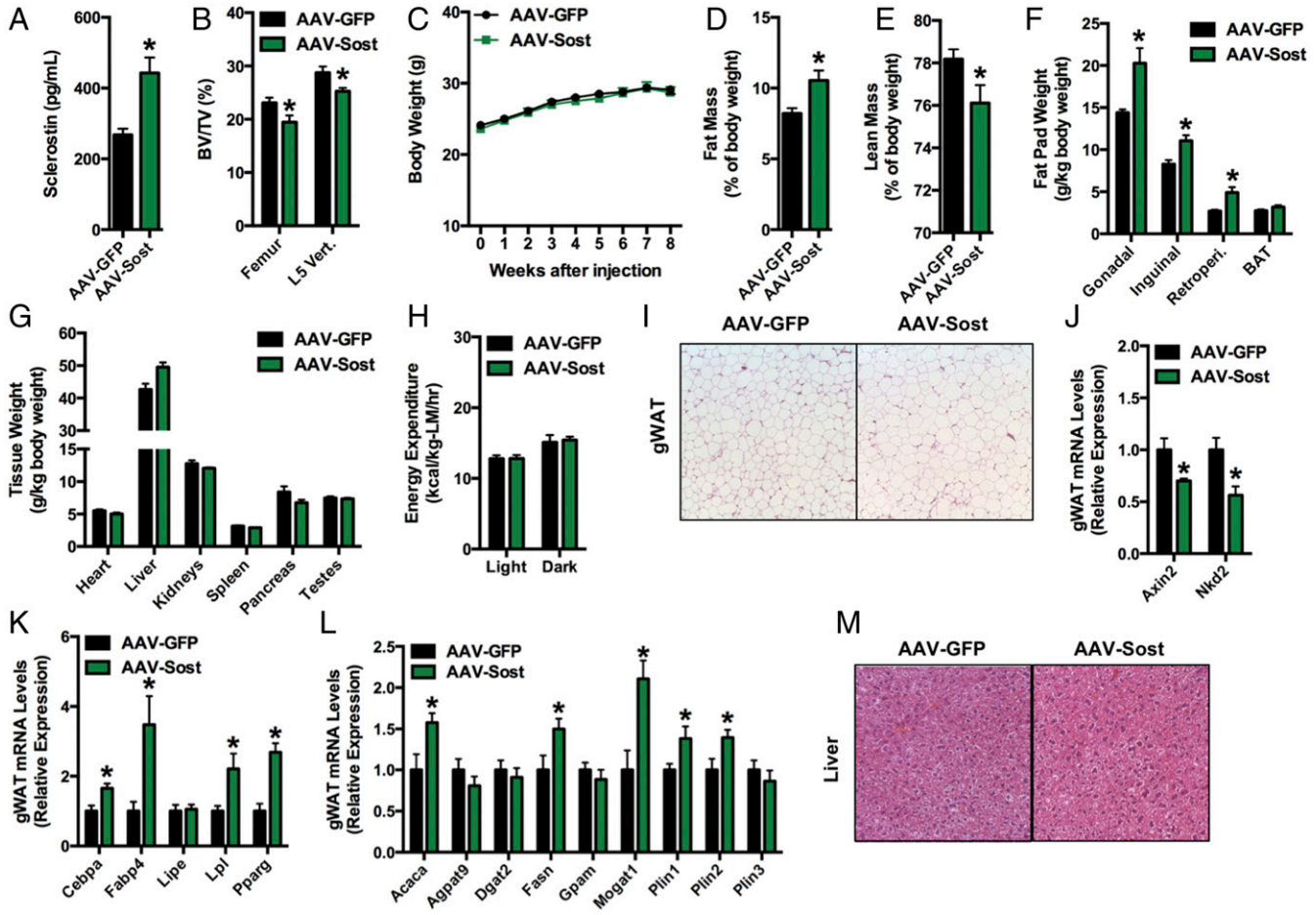

Fig. 2. Sclerostin overproduction increases fat mass. Eight-week-old C57BL/6 mice were injected with AAV8 constructs encoding *Sost* or GFP. (*A*) Serum sclerostin levels 8 wk after injection (n = 11–12 mice). (*B*) Quantification of trabecular bone volume in the distal femur and L5 vertebrae 8 wk after injection (n = 11–12 mice). (*C*) Body weight was assessed weekly (n = 8 mice). (*D* and *E*) qNMR analysis of fat mass and lean mass (n = 11–12 mice). (*F*) Adipose depot weights of AAV-GFP and AAV-Sost mice (n = 6–7 mice). (*G*) Wet tissue weights of major organs from AAV-GFP and AAV-Sost mice (n = 6–7 mice). (*H*) Energy expenditure from indirect calorimetry. Data are normalized to lean body mass (n = 6 mice). (*I*) Representative histological sections of the gonadal fat pad (gWAT) (10× magnification). (*J–L*) qPCR analysis of Wnt target gene (*J*), adipocyte differentiation markers (*K*), and lipid storage genes (*L*) in gWAT (n = 6 mice). (*M*) Representative histological sections of the liver (10× magnification). All data are represented as mean ± SEM. *$P < 0.05$.

a strong trend ($P = 0.06$) for increased insulin-stimulated glucose uptake in gonadal white adipose tissue (Fig. 3*M*). To verify this latter finding, we examined the acute phosphorylation of AKT and ERK after the administration of a bolus of insulin (Fig. 3 *N* and *O*), which confirmed an increase in insulin sensitivity in the gonadal fat pad of Sost$^{-/-}$ mice relative to controls.

By contrast, AAV-Sost mice exhibited deficiencies in parameters of glucose metabolism relative to controls. While glucose levels were normal (*SI Appendix*, Fig. S7*A*), serum insulin levels were significantly increased in AAV-Sost mice (*SI Appendix*, Fig. S7*B*) and the responses during glucose tolerance and insulin tolererance tests (*SI Appendix*, Fig. S7 *C–E*) were impaired relative to AAV-GFP mice. Pancreatic β-cell area per tissue area and islet size (*SI Appendix*, Fig. S7 *F–H*) were increased in AAV-Sost mice, and insulin sensitivity, assessed by AKT phosphorylation, was reduced in gonadal adipose tissue (*SI Appendix*, Fig. S7 *I* and *J*).

The increased insulin sensitivity of Sost$^{-/-}$ mice was not associated with changes in the serum levels of either leptin or adiponectin (*SI Appendix*, Table S2). Additionally, the levels of undercarboxylated osteocalcin (also referred to as Glu-osteocalcin) were similar in Sost$^{-/-}$ mice and control littermates even though total osteocalcin levels were increased in Sost$^{-/-}$ mice (likely the result of increased bone formation in this model) (29). However, alterations in insulin sensitivity in each of the mutant mouse models were associated with a concomitant change in serum nonesterified fatty acids (*SI Appendix*, Table S3), a marker of adipose tissue lipolysis. The levels of cholesterol, glycerol, and ketones were not affected in either model, but serum triglycerides were increased in AAV-Sost mice, possibly as a result of altered lipid utilization or synthesis. Taken together these data suggest sclerostin exerts corresponding effects on body composition and lipid and glucose metabolism, presumably by modulating insulin sensitivity in a number of tissues.

Sost$^{-/-}$ Mice Are Protected Against Diet-Induced Obesity. We next examined the response of control and Sost$^{-/-}$ mice to an obesogenic high fat diet (60% of calories from fat) since this insult results in an increase in serum sclerostin levels (*SI Appendix*, Fig. S1). Over the 10-wk study, Sost$^{-/-}$ mice gained significantly less weight (Fig. 4*A* and *SI Appendix*, Fig. S8*A*), accumulated less white adipose tissue (Fig. 4*B* and *SI Appendix*, Fig. S8*B*), and exhibited a metabolic profile that partially mirrored that evident in chow fed mutants. Compared with controls, the Sost$^{-/-}$ mice had improvements in glucose tolerance and insulin sensitivity in association with reductions in β-cell islet hypertrophy, random fed glucose, serum insulin, and free fatty acids (Fig. 4 *C–L* and *SI Appendix*, Fig. S8 *C* and *D*).

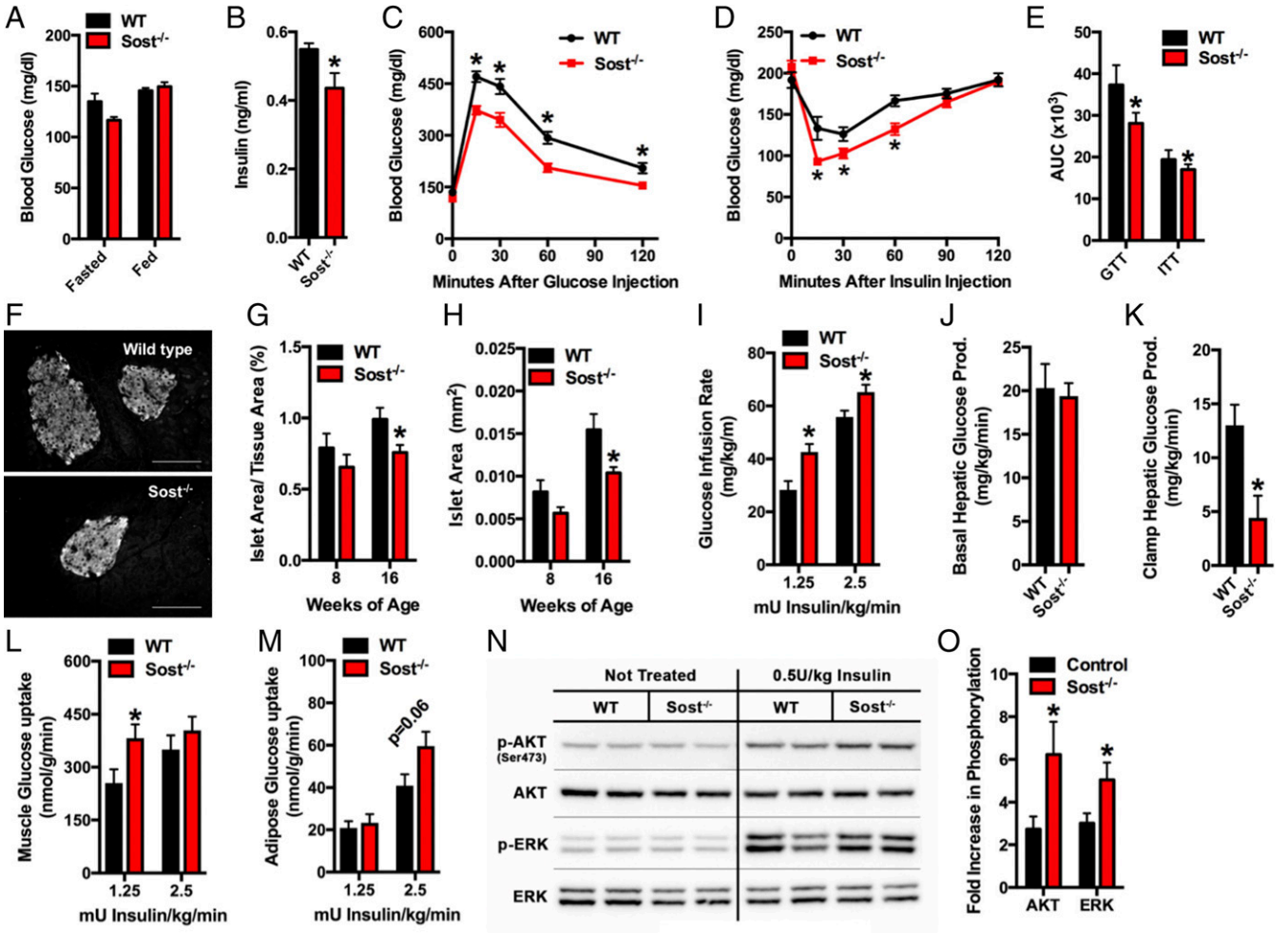

Fig. 3. Sclerostin modulates glucose metabolism in mice. (*A*) Fasting and random fed glucose in 16-wk-old control (WT) and Sost$^{-/-}$ mice (n = 8–14 mice). (*B*) Random fed insulin levels (n = 6–10 mice). (*C*) Glucose tolerance test (GTT) and (*D*) insulin tolerance test (ITT) at 16 wk of age (n = 6–8 mice). (*E*) Area under the curve (AUC) analysis for GTT and ITT. (*F*) Representative histological images of pancreatic islets after immunostaining for insulin at 16 wk of age (20× magnification). (*G* and *H*) Quantification of islet area per tissue area and mean islet area at 8 and 16 wk of age (n = 6 mice). (*I*) Steady-state glucose infusion rate, (*J*) basal hepatic glucose production, (*K*) clamp hepatic glucose production, (*L*) insulin-stimulated glucose uptake in skeletal muscle (gastrocnemius), and (*M*) white adipose tissue (gonadal) during hyperinsulinemic-euglycemic clamp performed on 16-wk-old control and Sost$^{-/-}$ mice (n = 6–8 mice). (*N*) Immunoblotting of phosphorylated AKT and ERK in gWAT before and after insulin stimulation. (*O*) Quantification of insulin-stimulated phosphorylation (n = 8–9 mice). All data are represented as mean ± SEM. *$P < 0.05$.

Notably, histological analysis of the gonadal fat pad revealed that in addition to maintaining smaller adipocytes (Fig. 4 *I* and *J*), Sost$^{-/-}$ mice did not develop the tissue inflammation that was evident in the gonadal fat pads of control mice (Fig. 4*I*). To confirm these observations, we profiled the expression of a number of genes associated with adipose tissue inflammation and oxidative stress by qPCR. In agreement with the histological analyses, the mRNA levels of inflammatory markers Ccl2, Ccl3, and Ccl4, as well as the oxidative stress genes Nox4, Sod1, and Sod2 were all significantly reduced in the fat pads of Sost$^{-/-}$ mice compared with controls (Fig. 4*K*). The expression of inflammatory markers was also reduced in the liver of HFD-fed Sost$^{-/-}$ mice (Fig. 4*N*), which accumulated lower levels of triglycerides (Fig. 4 *I* and *L*) and maintained a gene expression profile compatible with a reduction in hepatic steatosis (Fig. 4*M*). Thus, Sost$^{-/-}$ mice are resistant to the accumulation of body fat and maintain improvements in glucose and lipid metabolism even when challenged with a high fat diet. Moreover, sclerostin deficiency appears to limit inflammation in both the liver and white adipose tissue.

Sclerostin Regulates Adipocyte Metabolism and Differentiation. The consistent reduction in adipocyte size in Sost$^{-/-}$ mice, even in the face of high fat diet feeding, together with the adipocyte hypertrophy observed in AAV-Sost mice, led us to predict that these phenotypes were the result of changes in adipocyte metabolism. To address this hypothesis, we examined fatty acid metabolism by administering or incubating tissues with radiolabeled tracers. Compared with controls, fatty acid synthesis, indexed by the incorporation of ^{3}H-acetate into tissue lipids, was reduced by 53% and 52% in gWAT and iWAT, respectively (Fig. 5*A*). Similarly, the expression levels of enzymatic mediators of de novo fatty acid synthesis were decreased in the fat pads of Sost$^{-/-}$ mice relative to controls (*SI Appendix*, Fig. S9*A*). By contrast, long-chain fatty acid oxidation, assessed by measuring the conversion of 1-^{14}C-oleic acid to $^{14}CO_2$, was increased by 36% and 52% in gonadal and inguinal white adipose tissue isolated from Sost$^{-/-}$ mice, respectively (Fig. 5*B*). Further, the expression of genes associated with fatty acid oxidation and those typically associated with browning or beige adipocytes was up-regulated in parallel with a marker of activated Wnt signaling in both the gonadal and inguinal fat

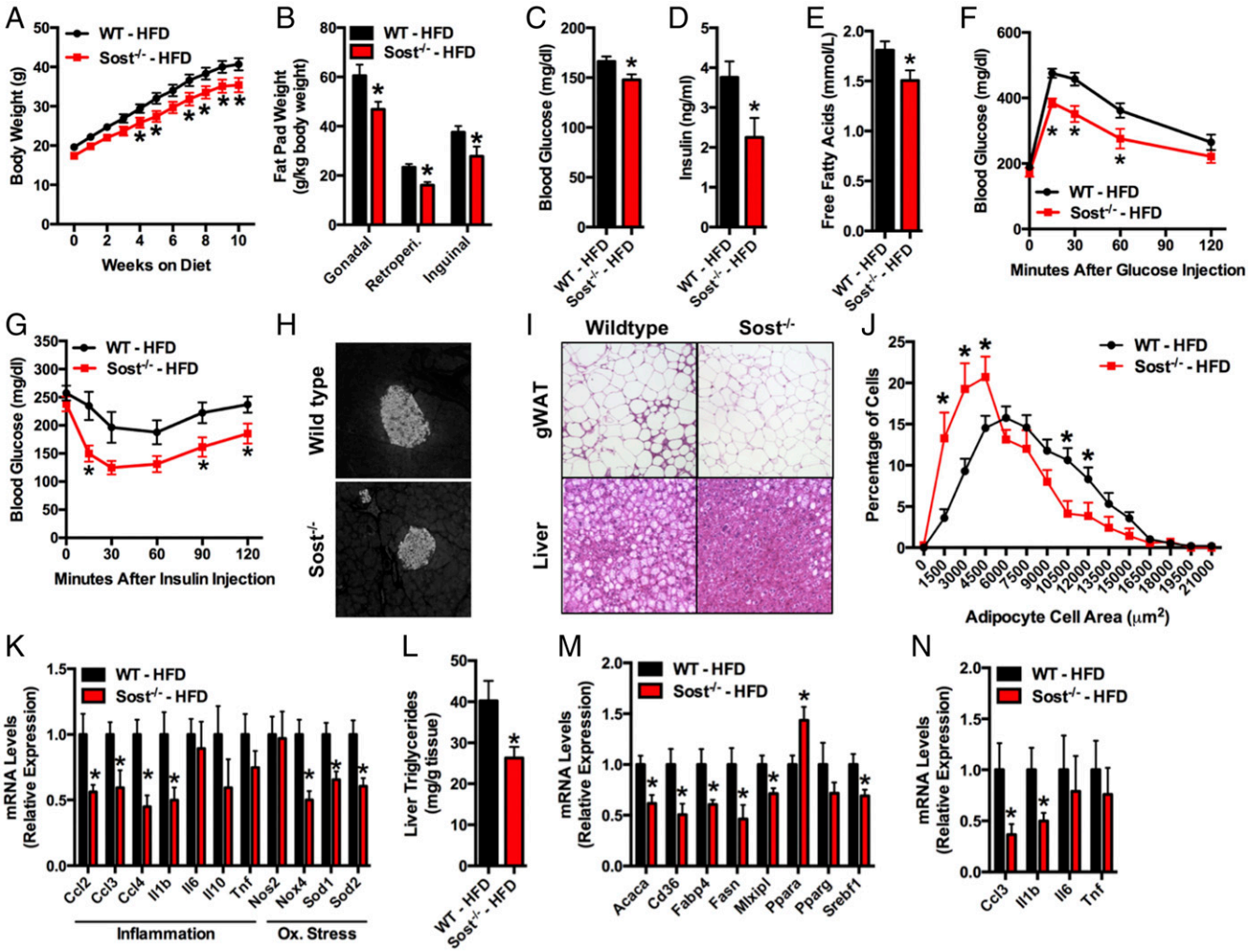

Fig. 4. Sost$^{-/-}$ mice are resistant to high fat diet feeding. Control (WT) and Sost$^{-/-}$ mice were fed a high fat diet (60% of calories from fat) from 6 wk of age. (*A*) Body weight was assessed weekly over the 10-wk study (n = 7–12 mice). (*B*) Adipose depot weights of high fat diet fed mice (n = 7–12 mice). (*C*) Random fed glucose levels (n = 7–12 mice). (*D*) Random fed insulin levels (n = 7–12 mice). (*E*) Serum-free fatty acids were assessed after 10 wk of high fat diet feeding (n = 7–12 mice). (*F*) Glucose tolerance testing and (*G*) insulin tolerance testing (n = 7–12 mice). (*H*) Representative histological images of pancreatic islets after immunostaining for insulin (20× magnification). (*I*) Representative histological sections of gonadal fat pad (gWAT) and liver after 10 wk of high fat diet feeding (10× magnification). (*J*) Frequency distribution of adipocyte size in the gonadal fat pad (n = 7–9 mice). (*K*) qPCR analysis of inflammatory and oxidative stress markers in the gonadal fat pad of high fat diet fed mice (n = 7–9 mice). (*L*) Assessment of liver triglycerides (n = 7–9 mice). (*M* and *N*) qPCR analsis of markers of steatosis and inflammation in the liver after high fat diet feeding (n = 7–9 mice). All data are represented as mean ± SEM. *P < 0.05.

pads of Sost$^{-/-}$ mice relative to control littermates (*SI Appendix*, Fig. S9 *B* and *C*). The up-regulation of Ucp1 and Ppargc1a in Sost$^{-/-}$ mice was confirmed by increases in positive immunostaining evident in histological sections of the inguinal fat pad (*SI Appendix*, Fig. S9*D*). Fatty acid metabolism in interscapular brown adipose and liver were not impacted by sclerostin deficiency (Fig. 5*B*).

As an in vitro counterpart to these studies, we examined the effects of recombinant mouse sclerostin on adipocyte differentiation since *Sost* gene transcripts are nearly undetectable in isolated white adipose tissue as well as primary mouse adipocytes and CD45^{-}, Sca1^{+}, Pdgfrα^{+} adipoprogenitors (41) (Fig. 5*C*), and adipocytes isolated from Sost$^{-/-}$ mice respond normally to Wnt ligand administration (Fig. 5*D*). Treating preadipocytes isolated from the inguinal fat pad with sclerostin augmented adipogenesis, which was marked by enhanced Oil Red O staining (Fig. 5*E*) and increases in the mRNA levels of Fabp4, Fasn, Plin1, Plin2, and Pparg (Fig. 5*F*). These findings agree with a recent study examining the effects of exogenous sclerostin on the 3T3-L1 adipocyte cell model (42). Importantly, recombinant sclerostin treatment also enhanced de novo lipid synthesis (Fig. 5*G*) and reduced both fatty acid oxidation (Fig. 5*H*) and the expression of genes associated with fatty acid catabolism (Fig. 5*I*).

Since Smad1/5/9 phosphorylation levels were reduced in the fat pads of Sost$^{-/-}$ mice (Fig. 1*K*), we examined whether sclerostin may regulate adipose tissue differentiation and metabolism by affecting adipogenic Bmp signaling (43–45). Consistent with this notion, mRNA levels for Bmp4 and Bmpr1a (Fig. 5*J*) and Smad1/5/9 phosphorylation levels (Fig. 5*K*) were increased in cultured primary adipocytes treated with recombinant sclerostin. Wnt3a treatment produced the opposite effect as the expression of Bmp4 and Bmpr1a were repressed (Fig. 5*J*). This finding was confirmed in vivo as Bmp4 and Bmpr1a expression were reduced in the gonadal fat pads of Sost$^{-/-}$ mice (Fig. 5*L*) and enhanced in those of AAV-Sost mice (Fig. 5*M*), relative to controls. Importantly, cotreatment of adipocyte cell cultures with the Bmp antagonist noggin, which did not affect Wnt signaling (Fig. 5*N*), completely abolished the increase in de

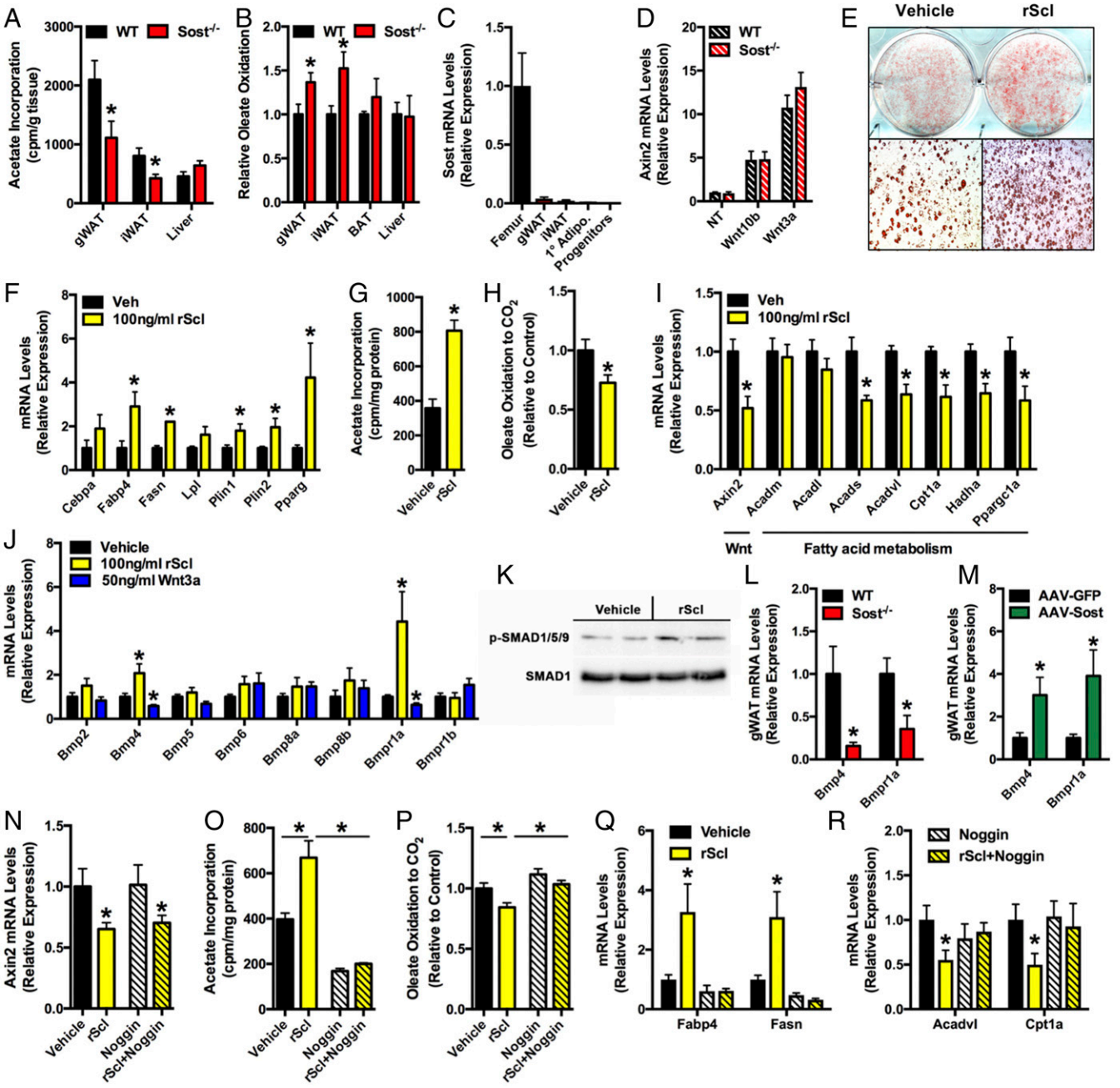

Fig. 5. Sclerostin regulates adipocyte metabolism by influencing Bmp4 expression. (*A*) De novo lipogeneis by gWAT, iWAT, and liver measured by the incorporation of ^{3}H-acetate into tissue lipids (n = 6–7 mice). (*B*) Relative levels of oleate oxidation by gWAT, iWAT, BAT, and liver assessed by measuring the conversion of 1-^{14}C-oleic acid to $^{14}CO_2$ (n = 4 mice). (*C*) qPCR analysis of Sost mRNA levels in femur, gWAT, iWAT, and primary mouse adipocytes, and CD45^{-}, Sca1^{+}, and Pdgfra^{+} adipoprogenitors (n = 5–6 mice). (*D*) qPCR analysis of Axin2 mRNA levels in primary mouse adipocytes isolated from WT and Sost$^{-/-}$ mice 6 h after stimulation with Wnt10b or Wnt3a. (*E*) Oil Red O staining of primary adipocyte cultures treated with vehicle or recombinant mouse sclerostin (100 ng/mL). (*F*) qPCR analysis of adipocyte differentiation markers. (*G*) 3H-acetate incorporation in primary mouse adipocytes treated with vehicle or recombinant mouse sclerostin. (*H*) Oleate oxidation by primary mouse adipocytes treated with vehicle or recombinant mouse sclerostin. (*I*) qPCR of Wnt target genes and mediators of fatty acid metabolism in primary mouse adipocytes treated with vehicle or recombinant sclerostin. (*J*) qPCR analysis of Bmp expression in primary mouse adipocytes treated with vehicle, recombinant sclerostin, or Wnt3a. (*K*) Immunoblot analysis of phosphorylated Smad1/5/9 levels in primary mouse adipocytes treated with vehicle or recombinant mouse sclerostin. (*L* and *M*) qPCR analysis of Bmp4 and Bmpr1a in gonadal adipose tissue isolated from Sost$^{-/-}$ mice (*L*) or AAV-Sost mice (*M*) and controls (n = 5–6 mice per group). (*N*–*R*) Primary mouse adipocytes were treated with vehicle, recominant mouse sclerostin (100 ng/mL), noggin (50 ng/mL), or a combination of the two. (*N*) qPCR analysis of Axin2 expression. (*O*) 3H-acetate incorporation. (*P*) Oleate oxidation. (*Q*) qPCR analysis of genes associated with adipocyte differentiation and fatty acid synthesis. (*R*) qPCR analysis of genes associated with fatty acid oxidation. In vitro studies were repeated in at least two independent experiments. All data are represented as mean ± SEM. *$P < 0.05$.

novo fatty acid synthesis (Fig. 5*O*) and reduction in fatty acid oxidation (Fig. 5*P*) prompted by sclerostin treatment, and disrupted sclerostin-induced alterations in the expression of genes associated with fatty acid synthesis (Fig. 5*Q*) and oxidation (Fig. 5*R*). Taken together, these data imply that increased Bmp signaling is downstream of sclerostin-mediated suppression of Wnt/β-catenin signaling in adipocytes and the regulation of adipocyte metabolism.

A Sclerostin-Neutralizing Antibody Influences Body Composition. Given the progression of anti-sclerostin therapeutics toward clinical use for the treatment of osteopenia/osteoporosis (46, 47), we questioned whether weekly administration of a sclerostin-neutralizing antibody (Scl Ab, 30 mg/kg) affects metabolism and the accumulation of body fat in wild-type mice fed a low or high fat diet. After 8 wk of treatment, Scl Ab had produced the expected anabolic response in the skeleton of mice fed either diet (*SI Appendix*, Table S4), increased the circulating levels of sclerostin as noted in previous studies (48) (Fig. 6*A*), and increased the expression of Axin2 in the femur as well as gWAT and iWAT (Fig. 6 *B* and *C*).

Consistent with high fat diet fed $Sost^{-/-}$ mice, we noted that Scl Ab-treated mice fed a high fat diet did not gain as much weight as vehicle-treated controls (Fig. 6*D*). qNMR analysis revealed a significant reduction in fat mass (Fig. 6*E*) and at necropsy the weights of white adipose tissue depots were reduced in Scl Ab-treated high fat diet fed mice (Fig. 6*H*). The body weights of Scl Ab-treated mice fed a low fat diet (LFD) were comparable to vehicle-treated controls, but the weights of fat pads were reduced (Fig. 6*G*). Lean mass (Fig. 6*F*) and lean tissue weights (*SI Appendix*, Fig. S10 *A* and *B*) were not affected by Scl Ab treatment, nor were food intake or energy expenditure (*SI Appendix*, Fig. S10 *C–F*).

Examination of tissue morphometry revealed that sclerostin neutralization mirrored the effect of *Sost* genetic deficiency as adipocyte size was reduced in both low fat diet and high fat diet fed mice (Fig. 6*I* and *SI Appendix*, Fig. S11 *A–D*). Moveover, gWAT and iWAT isolated from Scl Ab-treated mice exhibited an increased ability to oxidize 1-^{14}C-oleic acid to $^{14}CO_2$ (Fig. 6*J*) and maintained a gene expression profile compatible with increased fatty acid oxidation and reduced de novo synthesis (*SI Appendix*, Fig. S11 *E–J*). Serum glycerol and free fatty acid levels were reduced in Scl Ab-treated mice fed a low fat diet, while cholesterol levels were also reduced in high fat diet fed mice, relative to their respective controls (*SI Appendix*, Table S5). Fatty acid deposition in the liver of high fat diet fed mice also appeared to be reduced by Scl Ab treatment (Fig. 6*I*).

Scl Ab treatment also improved glucose handling. Mice fed a high fat diet receiving injections of the Scl Ab exhibited a reduction in random fed glucose levels (Fig. 6*K*) and treated mice on both diets maintained reduced levels of serum insulin (Fig. 6*L*). This effect is likely due to an increase in glucose and insulin tolerance (*SI Appendix*, Fig. S11 *K–N*) that leads to a reduction in pancreatic β-cell islet size (*SI Appendix*, Fig. S11 *O* and *P*). Taken together, these data indicated that in addition to the osteoanabolic effect, sclerostin neutralization prevents the accumulation of adipose tissue mass.

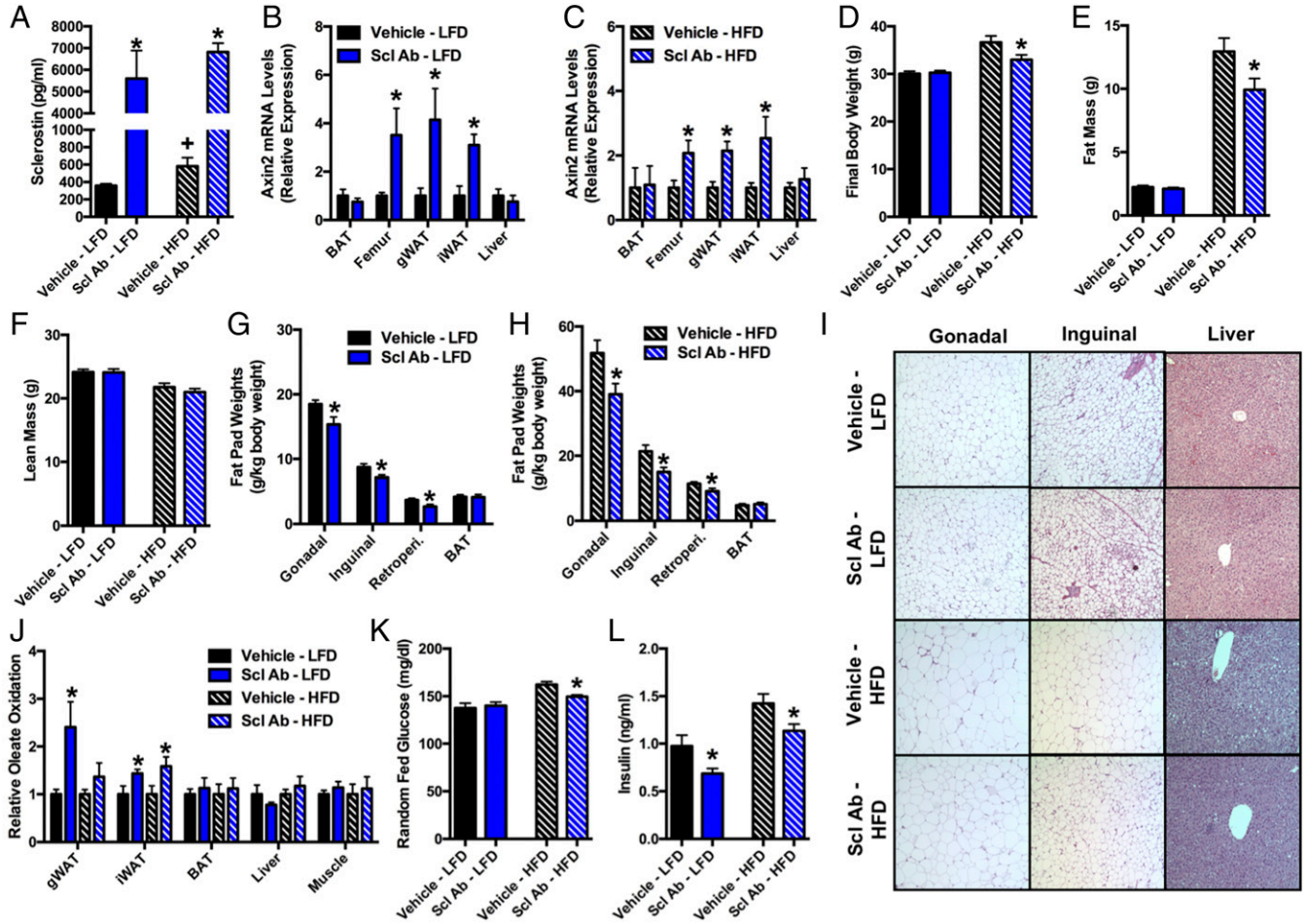

Fig. 6. Sclerostin-neutralizing antibodies reduce fat mass in mice. (*A*) Serum sclerostin levels in mice fed a low fat (LFD) or high fat diet (HFD) and treated weekly with vehicle or sclerostin-neutralizing antibody (Scl Ab, 30 mg/kg) for 8 wk (n = 8–10 mice per group). (*B* and *C*) qPCR analysis of Axin2 mRNA levels in tissues of vehicle or Scl Ab-treated mice fed LFD (*B*) or HFD (*C*) (n = 6 mice per group). (*D*) Final body weight after 8 wk on LFD or HFD (n = 8–10 mice per group). (*E* and *F*) qNMR analysis of fat mass and lean mass (n = 8–10 mice per group). (*G* and *H*) Adipose depot weights after 8 wk of treatment (n = 8–10 mice per group). (*I*) Representative histological sections of gonadal (gWAT) and inguinal (iWAT) fat pads and liver LFD- and HFD-fed mice treated with vehicle or Scl Ab (10× magnification). (*J*) Relative levels of oleate oxidation by gWAT, iWAT, BAT, liver, and muscle assessed by measuring the conversion of 1-^{14}C-oleic acid to $^{14}CO_2$ (n = 8–10 mice per group). (*K* and *L*) Random fed glucose and insulin levels for each treatment group (n = 8–10 mice per group). All data are represented as mean ± SEM. *$P < 0.05$.

Discussion

Due to its dramatic effects on bone acquisition (6, 7), sclerostin has almost exclusively been viewed as a local inhibitor of skeletal Wnt/β-catenin signaling. In this study, we uncovered a previously unexplored endocrine function for sclerostin. In accordance with the correlation of serum sclerostin levels with parameters of metabolic function in humans (17–24), sclerostin-deficient mice and those treated with a sclerostin-neutralizing antibody exhibit a reduction in the accumulation of white adipose tissue with corresponding enhancements in glucose handling and fatty acid metabolism. Mice that overproduce sclerostin as a result of adeno-associated virus gene transfer develop the reverse metabolic phenotype. We attribute these changes in metabolism to alterations in the metabolic function of white adipocytes.

The concept that Wnt/β-catenin signaling contributes to the coordination of cellular and whole-body metabolism can be traced to the initial studies describing the cloning of *LRP5* in humans, in which *LRP5* was identified as a candidate gene in the *IDDM4* locus that exhibited genetic linkage to insulin-dependent diabetes mellitus (49, 50). Subsequent studies have linked polymorphisms in *LRP5*, *LRP6*, Wnt ligands, and the downstream transcription factor *TCF7L2* to the development of metabolic disease in humans (26, 51–54). Adipocyte physiology is particularly sensitive to Wnt signaling. Wnt ligands are produced by preadipocytes, and their expression levels or downstream signaling must be suppressed to initiate adipogenesis (33). In this regard, mice that are genetically engineered for increased Wnt signaling in adipocytes via the overexpression of Wnt10b develop a phenotype that is remarkably similar to that which we observed in $Sost^{-/-}$ mice, including a reduction in fat mass, resistance to diet-induced obesity, and improvements in glucose metabolism (34). Likewise, β-catenin has been shown previously to interact with and inhibit the activity of Pparγ (55), and maturing adipocytes produce secreted Wnt inhibitors that sequester ligands and promote the attainment of a mature phenotype (30, 56). Since *Sost* mRNAs are nearly undetectable in adipose tissue, primary adipocytes, and adipoprogenitors and adipocytes isolated from $Sost^{-/-}$ mice respond normally to a Wnt stimulus, our data imply that bone-derived sclerostin acts on white adipose via a cell nonautonomous mechanism.

White adipose tissue isolated from $Sost^{-/-}$ mice and those receiving the Scl Ab exhibit increased oxidation of fatty acids and corresponding increases in the expression of enzymatic mediators of fatty acid utilization. Conversely, measures of fatty acid synthesis were dramatically reduced in gWAT and iWAT isolated from $Sost^{-/-}$ mice. Together these in vivo data indicate that sclerostin regulates both anabolic and catabolic pathways of metabolism, which in turn leads to an overall increase in fat mass and adipocyte size. Our in vitro findings of repressed long-chain fatty acid oxidation and enhanced fatty acid synthesis after recombinant sclerostin treatment further support this idea. Moreover, these data accord with recent findings that indicate Wnt signaling directly regulates metabolic capacity in other tissues, including liver and bone (57, 58), and resemble the phenotype of mice lacking secreted-frizzled related protein 5 (Sfrp5), a secreted inhibitor of Wnt signaling produced by adipocytes. Much like $Sost^{-/-}$ mice, genetic ablation of Sfrp5 expression suppresses adipocyte hypertrophy and increases metabolic capacity of adipocytes (30).

The observation that fat mass is altered in $Sost^{-/-}$ mice as well as those overproducing Sost (AAV-Sost) without a corresponding change in whole body energy expenditure is counterintuitive but not surprising. Adipose tissue contributes only a small fraction (1–2% of that contributed by the heart, kidney, and liver) to the resting metabolic rate (31, 59). Therefore, the alterations in fatty acid synthesis and catabolism in Sost knockout and overexpressing mice, which produced changes in adipose tissue mass over the life of the animals, may not be sufficient to produce a detectable change in energy expenditure in indirect calorimetry studies. In agreement with this interpretation, Sfrp5 mutant mice also do not exhibit a change in energy expenditure despite an increase in adipocyte mitochondrial content (30). Moreover, Lee et al. (32) recently reported that mice lacking Cpt2, an obligate enzyme in long-chain fatty acid catabolism, specifically in white and brown adipose tissue (BAT), develop increased adipose tissue mass without changes in energy expenditure. A reduction in whole-body oxidative metabolism was only evident in this model when challenged by cold exposure or β-adrenergic stimulation (32). The increased prevalence of Ppargc1α and Ucp1 mRNA and protein in white adipose tissue depots raises the possibility that a similar stimulus may be necessary to increase whole-body energy expenditure in $Sost^{-/-}$ mice. Confirming this hypothesis will require additional studies.

Mechanistically, our data suggest that sclerostin exerts its effects on adipocyte metabolism by indirectly regulating Bmp signaling. Early mechanistic studies on the action of sclerostin suggested it might act as a Bmp antagonist (37), but the abundance of genetic and pharmacological data indicate that it primarily functions as an inhibitor of Wnt signaling (5, 8). As expected, markers of Wnt signaling were increased in the white adipose tissue of $Sost^{-/-}$ mice, but indicators of Bmp signaling were reduced. Consistent with this observation, the expression levels of Bmp4 and its receptor Bmpr1a were negatively correlated with the levels of Wnt signaling in adipocytes both in vitro and in vivo and the Bmp antagonist noggin abolished the effects of recombinant sclerostin on adipocyte metabolism in vitro. These data align with the established cross-talk among the Wnt and Bmp pathways, the adipogenic effects of Bmp signaling (43–45), and a recent study which indicates that Bmp4 facilitates adipocyte hypertrophy by enhancing fatty acid synthesis and suppressing oxidation (45).

The hyperinsulinemic-euglycemic clamp studies performed on Sost mutants and their control littermates indicated that in addition to affecting adipocyte physiology, sclerostin can influence insulin sensitivity in the liver and skeletal muscle. This finding was somewhat surprising since *Sost* deficiency did not result in a change in Wnt-target gene expression in these tissues, but accords with the correlation between serum sclerostin levels and fasting glucose production and hepatic insulin sensitivity observed in humans (24). Dissecting the molecular basis for the increased insulin sensitivity in the liver and muscle of $Sost^{-/-}$ mice will require additional study, but this may represent an indirect effect. Indeed, Zeve et al. (60) demonstrated that activation of Wnt signaling in adipose tissue stimulates the release of a circulating factor that increases glucose uptake in skeletal muscle.

If the endocrine functions of sclerostin described here in mouse models extend to humans, which seems likely, given the clinical correlations cited above, the results of our study are likely to have an important impact on therapeutics that target Wnt signaling. Enhancing adipocyte metabolism and the induction of a beige adipocyte phenotype within white adipose tissue is considered to be a promising strategy for the treatment of obesity and related metabolic diseases due to the ability of these specialized cells to metabolize glucose and fatty acids and dissipate energy as heat. Our data demonstrate that a sclerostin-neutralizing antibody is sufficient to increase bone mass and concomitantly reduce adipose tissue mass, which raises the possibility that this therapeutic paradigm may produce an off-target but beneficial outcome. Sclerostin neutralization might prove to be an effective treatment for two epidemic disorders: osteopenia/osteoporosis and obesity. However, to the best of our knowledge, changes in body composition, insulin sensitivity, or fatty acid metabolism have not been an outcome in the ongoing human studies.

Materials and Methods

The Institutional Animal Care and Use Committee of Johns Hopkins University approved all procedures involving mice. All mice were maintained on a C57BL/6 background and obtained from The Jackson Laboratory unless specificed otherwise. $Sost^{-/-}$ mice ($Sost^{tm1(KOMP)Vlcg}$) were obtained from the

KOMP Repository (www.komp.org/) and originally created by Regeneron Pharmaceuticals, Inc. using ES cell clone 10069B-C10. Methods used to create the Velocigene target allele have been reported previously (61). For Sost overexpression studies, adenoviruses (AAV8-CMV) encoding mouse Sost or green fluorescent protein were obtained from Vector Biolabs. Sclerostin-neutralizing antibody (30 mg/kg; Eli Lilly) or vehicle was delivered weekly by s.c. injection. The hyperinsulinemic-euglycemic clamp was conducted at the National Mouse Metabolic Phenotyping Center at the University of Massachusetts Medical School. Please see the *SI Appendix, SI Materials and Methods* for additional experimental details. All results are presented as means ± SEs of the mean. Statistical analyses were performed using unpaired, two-tailed Student's *t* or ANOVA tests followed by post hoc tests. A *P* value less that 0.05 was considered significant. In all figures, $*P \leq 0.05$.

ACKNOWLEDGMENTS. This work was supported by Merit Review Grant BX003724 from the Biomedical Laboratory Research and Development Service of the Veterans Affairs Office of Research and Development (to R.C.R.), NIH Grants DK099134 (to R.C.R.) and NS072241 (to M.J.W.), and NIH Grant DK079637 to the Baltimore Diabetes Research Center (M.A.H. and R.C.R.). Part of this study was performed at the National Mouse Metabolic Phenotyping Center at the University of Massachusetts Medical School and funded by NIH Grant U2C-DK093000.

1. Fazeli PK, Klibanski A (2014) Anorexia nervosa and bone metabolism. *Bone* 66:39–45.
2. Nussbaum M, Baird D, Sonnenblick M, Cowan K, Shenker IR (1985) Short stature in anorexia nervosa patients. *J Adolesc Health Care* 6:453–455.
3. DiGirolamo DJ, Clemens TL, Kousteni S (2012) The skeleton as an endocrine organ. *Nat Rev Rheumatol* 8:674–683.
4. Karsenty G, Ferron M (2012) The contribution of bone to whole-organism physiology. *Nature* 481:314–320.
5. Moester MJ, Papapoulos SE, Löwik CW, van Bezooijen RL (2010) Sclerostin: Current knowledge and future perspectives. *Calcif Tissue Int* 87:99–107.
6. Balemans W, et al. (2001) Increased bone density in sclerosteosis is due to the deficiency of a novel secreted protein (SOST). *Hum Mol Genet* 10:537–543.
7. Balemans W, et al. (2002) Identification of a 52 kb deletion downstream of the SOST gene in patients with van Buchem disease. *J Med Genet* 39:91–97.
8. Burgers TA, Williams BO (2013) Regulation of Wnt/β-catenin signaling within and from osteocytes. *Bone* 54:244–249.
9. Veverka V, et al. (2009) Characterization of the structural features and interactions of sclerostin: Molecular insight into a key regulator of Wnt-mediated bone formation. *J Biol Chem* 284:10890–10900.
10. Li X, et al. (2005) Sclerostin binds to LRP5/6 and antagonizes canonical Wnt signaling. *J Biol Chem* 280:19883–19887.
11. Semënov M, Tamai K, He X (2005) SOST is a ligand for LRP5/LRP6 and a Wnt signaling inhibitor. *J Biol Chem* 280:26770–26775.
12. Arasu A, et al.; Study of Osteoporotic Fractures Research Group (2012) Serum sclerostin and risk of hip fracture in older Caucasian women. *J Clin Endocrinol Metab* 97:2027–2032.
13. Ardawi MS, et al. (2012) High serum sclerostin predicts the occurrence of osteoporotic fractures in postmenopausal women: The center of excellence for osteoporosis research study. *J Bone Miner Res* 27:2592–2602.
14. Mödder UI, et al. (2011) Relation of age, gender, and bone mass to circulating sclerostin levels in women and men. *J Bone Miner Res* 26:373–379.
15. Mödder UI, et al. (2011) Regulation of circulating sclerostin levels by sex steroids in women and in men. *J Bone Miner Res* 26:27–34.
16. Drake MT, et al. (2010) Effects of parathyroid hormone treatment on circulating sclerostin levels in postmenopausal women. *J Clin Endocrinol Metab* 95:5056–5062.
17. García-Martín A, et al. (2012) Circulating levels of sclerostin are increased in patients with type 2 diabetes mellitus. *J Clin Endocrinol Metab* 97:234–241.
18. Gennari L, et al. (2012) Circulating sclerostin levels and bone turnover in type 1 and type 2 diabetes. *J Clin Endocrinol Metab* 97:1737–1744.
19. Gaudio A, et al. (2012) Sclerostin levels associated with inhibition of the Wnt/β-catenin signaling and reduced bone turnover in type 2 diabetes mellitus. *J Clin Endocrinol Metab* 97:3744–3750.
20. Urano T, Shiraki M, Ouchi Y, Inoue S (2012) Association of circulating sclerostin levels with fat mass and metabolic disease: Related markers in Japanese postmenopausal women. *J Clin Endocrinol Metab* 97:E1473–E1477.
21. Amrein K, et al. (2012) Sclerostin and its association with physical activity, age, gender, body composition, and bone mineral content in healthy adults. *J Clin Endocrinol Metab* 97:148–154.
22. Sheng Z, et al. (2012) Serum sclerostin levels were positively correlated with fat mass and bone mineral density in central south Chinese postmenopausal women. *Clin Endocrinol (Oxf)* 76:797–801.
23. Ma YH, et al. (2014) Circulating sclerostin associated with vertebral bone marrow fat in older men but not women. *J Clin Endocrinol Metab* 99:E2584–E2590.
24. Daniele G, et al. (2015) Sclerostin and insulin resistance in prediabetes: Evidence of a cross talk between bone and glucose metabolism. *Diabetes Care* 38:1509–1517.
25. Semenov MV, He X (2006) LRP5 mutations linked to high bone mass diseases cause reduced LRP5 binding and inhibition by SOST. *J Biol Chem* 281:38276–38284.
26. Loh NY, et al. (2015) LRP5 regulates human body fat distribution by modulating adipose progenitor biology in a dose- and depot-specific fashion. *Cell Metab* 21:262–272.
27. Wei P, Lane PH, Lane JT, Padanilam BJ, Sansom SC (2004) Glomerular structural and functional changes in a high-fat diet mouse model of early-stage type 2 diabetes. *Diabetologia* 47:1541–1549.
28. Cejka D, et al. (2014) Renal elimination of sclerostin increases with declining kidney function. *J Clin Endocrinol Metab* 99:248–255.
29. Li X, et al. (2008) Targeted deletion of the sclerostin gene in mice results in increased bone formation and bone strength. *J Bone Miner Res* 23:860–869.
30. Mori H, et al. (2012) Secreted frizzled-related protein 5 suppresses adipocyte mitochondrial metabolism through WNT inhibition. *J Clin Invest* 122:2405–2416.
31. Wang Z, et al. (2010) Specific metabolic rates of major organs and tissues across adulthood: Evaluation by mechanistic model of resting energy expenditure. *Am J Clin Nutr* 92:1369–1377.
32. Lee J, Ellis JM, Wolfgang MJ (2015) Adipose fatty acid oxidation is required for thermogenesis and potentiates oxidative stress-induced inflammation. *Cell Rep* 10:266–279.
33. Bennett CN, et al. (2002) Regulation of Wnt signaling during adipogenesis. *J Biol Chem* 277:30998–31004.
34. Longo KA, et al. (2004) Wnt10b inhibits development of white and brown adipose tissues. *J Biol Chem* 279:35503–35509.
35. Jho EH, et al. (2002) Wnt/beta-catenin/Tcf signaling induces the transcription of Axin2, a negative regulator of the signaling pathway. *Mol Cell Biol* 22:1172–1183.
36. Yan D, et al. (2001) Elevated expression of axin2 and hnkd mRNA provides evidence that Wnt/beta-catenin signaling is activated in human colon tumors. *Proc Natl Acad Sci USA* 98:14973–14978.
37. Winkler DG, et al. (2003) Osteocyte control of bone formation via sclerostin, a novel BMP antagonist. *EMBO J* 22:6267–6276.
38. Collette NM, et al. (2013) Sost and its paralog Sostdc1 coordinate digit number in a Gli3-dependent manner. *Dev Biol* 383:90–105.
39. Kim JI, et al. (2015) Lipid-overloaded enlarged adipocytes provoke insulin resistance independent of inflammation. *Mol Cell Biol* 35:1686–1699.
40. Salans LB, Knittle JL, Hirsch J (1968) The role of adipose cell size and adipose tissue insulin sensitivity in the carbohydrate intolerance of human obesity. *J Clin Invest* 47:153–165.
41. Hepler C, Vishvanath L, Gupta RK (2017) Sorting out adipocyte precursors and their role in physiology and disease. *Genes Dev* 31:127–140.
42. Ukita M, Yamaguchi T, Ohata N, Tamura M (2016) Sclerostin enhances adipocyte differentiation in 3T3-L1 cells. *J Cell Biochem* 117:1419–1428.
43. Tang QQ, Otto TC, Lane MD (2004) Commitment of C3H10T1/2 pluripotent stem cells to the adipocyte lineage. *Proc Natl Acad Sci USA* 101:9607–9611.
44. Huang H, et al. (2009) BMP signaling pathway is required for commitment of C3H10T1/2 pluripotent stem cells to the adipocyte lineage. *Proc Natl Acad Sci USA* 106:12670–12675.
45. Modica S, et al. (2016) Bmp4 promotes a brown to white-like adipocyte shift. *Cell Rep* 16:2243–2258.
46. Cosman F, et al. (2016) Romosozumab treatment in postmenopausal women with osteoporosis. *N Engl J Med* 375:1532–1543.
47. McClung MR, et al. (2014) Romosozumab in postmenopausal women with low bone mineral density. *N Engl J Med* 370:412–420.
48. Yee CS, et al. (2016) Sclerostin antibody treatment improves fracture outcomes in a type I diabetic mouse model. *Bone* 82:122–134.
49. Twells RC, et al. (2001) The sequence and gene characterization of a 400-kb candidate region for IDDM4 on chromosome 11q13. *Genomics* 72:231–242.
50. Hey PJ, et al. (1998) Cloning of a novel member of the low-density lipoprotein receptor family. *Gene* 216:103–111.
51. Guo YF, et al. (2006) Polymorphisms of the low-density lipoprotein receptor-related protein 5 (LRP5) gene are associated with obesity phenotypes in a large family-based association study. *J Med Genet* 43:798–803.
52. Christodoulides C, et al. (2006) WNT10B mutations in human obesity. *Diabetologia* 49:678–684.
53. Grant SF, et al. (2006) Variant of transcription factor 7-like 2 (TCF7L2) gene confers risk of type 2 diabetes. *Nat Genet* 38:320–323.
54. Tomaszewski M, et al. (2009) A common variant in low-density lipoprotein receptor-related protein 6 gene (LRP6) is associated with LDL-cholesterol. *Arterioscler Thromb Vasc Biol* 29:1316–1321.
55. Liu J, Wang H, Zuo Y, Farmer SR (2006) Functional interaction between peroxisome proliferator-activated receptor gamma and beta-catenin. *Mol Cell Biol* 26:5827–5837.
56. Christodoulides C, et al. (2006) The Wnt antagonist dickkopf-1 and its receptors are coordinately regulated during early human adipogenesis. *J Cell Sci* 119:2613–2620.
57. Frey JL, et al. (2015) Wnt-Lrp5 signaling regulates fatty acid metabolism in the osteoblast. *Mol Cell Biol* 35:1979–1991.
58. Boj SF, et al. (2012) Diabetes risk gene and Wnt effector Tcf7l2/TCF4 controls hepatic response to perinatal and adult metabolic demand. *Cell* 151:1595–1607.
59. Elia M (1992) Organ and tissue contribution to metabolic rate. *Energy Metabolism: Tissue Determinants and Cellular Corollaries*, eds Kinney JM, Tucker HN (Raven Press, New York), pp 61–80.
60. Zeve D, et al. (2012) Wnt signaling activation in adipose progenitors promotes insulin-independent muscle glucose uptake. *Cell Metab* 15:492–504.
61. Valenzuela DM, et al. (2003) High-throughput engineering of the mouse genome coupled with high-resolution expression analysis. *Nat Biotechnol* 21:652–659.